Biointerface Research in Applied Chemistry
Open-Access Journal (ISSN: 2069-5837)

Article
Volume 16, Issue 4, 2026, 107
https://doi.org/10.33263/BRIAC164.107

Bioactive Compounds from Sungkai Leaves (*Peronema canescens*) as Candidate Allosteric Modulators of Superoxide Dismutase: An *In silico* Study

R. Haryo Bimo Setiarto [1,*], Muhammad Marsha Azzami Hasibuan [2], Dimas Andrianto [2]

[1] Research Center for Applied Microbiology, National Research and Innovation Agency (BRIN), KST Soekarno, Cibinong, Bogor, 16911, Indonesia; rhar002@brin.go.id (R.H.B.S.);
[2] Department of Biochemistry, IPB University, Bogor, 16680, Indonesia; marshaazzami@apps.ipb.ac.id (M.M.A.H.); dimasandrianto@apps.ipb.ac.id (D.A.);
* Correspondence: rhar002@brin.go.id;

Received: 19.03.2026; Accepted: 26.05.2026; Published: 15.08.2026

Abstract: Bioactive compounds derived from medicinal plants have attracted considerable scientific interest because of their diverse biochemical properties and potential antioxidant-related activities. *Peronema canescens* is traditionally used in herbal medicine and contains phytochemical constituents with potential biological activity. In this study, an *in silico* approach was used to evaluate bioactive compounds from sungkai leaves for their potential to modulate superoxide dismutase (SOD) allosterically. This important antioxidant enzyme protects against oxidative stress. The study included Lipinski screening, bioavailability prediction, toxicity prediction, and molecular docking analysis targeting the predicted allosteric region of SOD. In addition, global and local chemical reactivity descriptors and bioactivity-related properties were analyzed to support preliminary structure–activity relationship (SAR) assessment. Among the screened compounds, CHEMBL1407860 demonstrated acceptable predicted pharmacokinetic and toxicity profiles. It showed a higher docking score at the predicted allosteric site of SOD than D-trehalose (6.128 kcal/mol vs 5.183 kcal/mol) within the YASARA scoring framework. Residue-interaction analysis indicated potential binding interactions near the enzyme's predicted allosteric region. However, these findings are based solely on computational prediction and do not confirm enzymatic activation or therapeutic efficacy. Therefore, CHEMBL1407860 may be considered a computationally prioritized candidate for further investigation as a possible SOD allosteric-binding compound. Additional molecular dynamics simulations, biochemical enzyme assays, and cellular studies are required to validate its biological activity and mechanism of action.

Keywords: allostery; molecular docking; sungkai; superoxide dismutase; YASARA.

1. Introduction

Plant-derived bioactive compounds have attracted considerable scientific interest because of their diverse biochemical activities and potential health benefits. Numerous studies have reported that plant-based diets and phytochemical-rich natural products may help protect against chronic diseases such as cardiovascular disorders, diabetes mellitus, neurodegenerative diseases, obesity, and cancer by modulating oxidative stress and inflammatory pathways [1]. Oxidative stress occurs when the production of reactive oxygen species (ROS) exceeds the

antioxidant defense capacity of biological systems, leading to cellular damage involving lipids, proteins, and nucleic acids [2]. Among ROS, the superoxide radical anion (O^{2-}) is one of the primary reactive species generated during cellular metabolism and pathological stress conditions.

Antioxidant defense systems consist of enzymatic and non-enzymatic components that cooperate to maintain cellular redox homeostasis. Enzymatic antioxidants include superoxide dismutase (SOD), catalase, and glutathione peroxidase. Among these enzymes, SOD is considered one of the most important first-line antioxidant defense enzymes because it catalyzes the dismutation of superoxide radicals into hydrogen peroxide and molecular oxygen, thereby reducing the accumulation of highly reactive superoxide species [3]. Cytosolic Cu/Zn-SOD (SOD1; EC 1.15.1.1) plays a critical role in protecting cells against oxidative injury through cyclic oxidation–reduction reactions involving copper ions at the catalytic center [4].

In recent years, interest has increased not only in direct radical-scavenging antioxidants but also in compounds that modulate endogenous antioxidant enzymes, such as SOD. Activation or stabilization of SOD may provide therapeutic advantages, as endogenous antioxidant enzymes can act continuously within physiological antioxidant networks and offer more sustained protection against oxidative stress than transient exogenous antioxidants. SOD modulation has therefore been investigated in relation to aging, neurodegenerative disorders, inflammatory diseases, metabolic syndrome, and cardiovascular dysfunction [5,6]. However, modulation of antioxidant enzymes must be carefully regulated because excessive or nonspecific activation of SOD may alter cellular redox balance and potentially increase hydrogen peroxide accumulation, which may contribute to oxidative signaling dysregulation if not efficiently removed by downstream antioxidant systems such as catalase and glutathione peroxidase [7]. Therefore, selective and controlled modulation of SOD remains an important research objective.

Recent advances in computational biology and chemoinformatics have enabled the identification of potential enzyme modulators through molecular docking, pharmacokinetic prediction, toxicity screening, and allosteric-site analysis. In particular, allosteric modulation has emerged as an attractive strategy in drug discovery because allosteric ligands can regulate enzyme activity without directly competing with endogenous substrates at the catalytic site [8]. Nevertheless, computational screening approaches remain predictive and hypothesis-generating, and docking interactions alone cannot confirm functional activation or biological efficacy without experimental validation [9].

One medicinal plant receiving increasing ethnopharmacological attention is Peronema canescens, a tropical species in the family Verbenaceae. Sungkai has traditionally been used by local communities, including the Dayak ethnic group, to treat fever, influenza, skin disorders, stomach pain, and inflammatory conditions [10]. Previous phytochemical investigations have reported that sungkai leaves contain flavonoids, phenolic compounds, terpenoids, alkaloids, tannins, and other secondary metabolites associated with antioxidant and pharmacological activities [11–13]. Several studies have also demonstrated antioxidant, antidiabetic, antibacterial, antihypertensive, and anti-inflammatory properties of sungkai extracts, suggesting that its bioactive constituents may influence oxidative-stress-related biological pathways [14–16].

Based on these considerations, the present study employed an *in silico* computational approach to investigate bioactive compounds derived from Peronema canescens leaves as potential modulators of superoxide dismutase. The study included Lipinski screening,

bioavailability prediction, ADMET and toxicity analyses, allosteric site prediction, and molecular docking against SOD. In addition, global and local chemical reactivity descriptors, predicted biochemical targets, and bioactivity-related properties were evaluated to support preliminary structure–activity relationship (SAR) analysis [17-19]. The objective of this study was not to confirm enzymatic activation, but rather to prioritize candidate compounds for further biochemical and pharmacological investigation computationally.

2. Materials and Methods

2.1. Materials and software.

This computational study was performed on a Windows 11 Professional 64-bit computer with an AMD Ryzen 5 5600H processor (3.30–4.20 GHz). Molecular modeling and visualization analyses were conducted using Yet Another Scientific Artificial Reality Application (YASARA Structure), BIOVIA Discovery Studio Visualizer, and PyMOL software. Bioactive compounds from Peronema canescens leaves were identified from the phytochemical literature and verified in the PubChem database (https://pubchem.ncbi.nlm.nih.gov). Protein structural data were obtained from the Research Collaboratory for Structural Bioinformatics Protein Data Bank (RCSB PDB) (https://www.rcsb.org). A total of 42 phytochemical compounds reported from sungkai leaves were included in the screening analysis, as provided in Supplementary Table S1.

2.2. Protein functional sites and allosteric-site identification.

Functional-site analysis of the target protein was performed using the Conserved Domain Database (CDD) search tool available through the CD-Search web server (https://www.ncbi.nlm.nih.gov/Structure/cdd/wrpsb.cgi) [11,13]. The analyses included identification of active-site residues, substrate-binding regions, and metal-binding residues associated with Cu^{2+} and Zn^{2+} coordination. Prediction of potential allosteric sites was performed using the Allosteric Database (ASD; https://mdl.shsmu.edu.cn/ASD) and AllositePro server (https://mdl.shsmu.edu.cn/AST/) [10,15]. Predicted pockets were evaluated based on pocket volume, residue composition, druggability score, and spatial proximity to known catalytic and structural regions. The selected docking pocket had the highest predicted allosteric confidence score and was located adjacent to residues involved in the conformational regulation of the SOD structure.

2.3. Pharmacokinetic test and ADMET prediction.

Pharmacokinetic evaluation was conducted to estimate the drug-likeness and ADMET properties of the screened compounds. Molecular structures in SMILES format were analyzed using SwissADME (http://www.swissadme.ch; accessed January 2026) [1,12,14], pkCSM (https://biosig.lab.uq.edu.au/pkcsm/prediction; accessed January 2026), and Deep-PK (https://biosig.lab.uq.edu.au/deeppk/; accessed January 2026) [1,12]. The evaluated parameters included molecular weight, lipophilicity (LogP), hydrogen-bond donor and acceptor counts, topological polar surface area (TPSA), gastrointestinal absorption, blood–brain barrier permeability, cytochrome P450 interactions, total clearance, and bioavailability predictions. Drug-likeness screening was primarily assessed according to Lipinski's Rule of Five criteria: molecular weight ≤500 Da, LogP ≤5, hydrogen-bond donors ≤5, hydrogen-bond acceptors ≤10,

and TPSA ≤140 Å². Compounds violating one or more criteria were recorded and interpreted individually rather than automatically excluded. Cross-comparison among SwissADME, pkCSM, and Deep-PK outputs was performed to improve consistency of pharmacokinetic interpretation. However, all ADMET results were considered predictive and exploratory because these computational models have limitations in their applicability domains, training datasets, and structural generalization.

2.4. Toxicity prediction.

Toxicity prediction of the screened compounds was performed using ProTox-III (https://tox.charite.de/protox3; accessed January 2026). Toxicological endpoints included predicted oral toxicity (LD50), toxicity class, hepatotoxicity, carcinogenicity, immunotoxicity, mutagenicity, and cytotoxicity. The server's prediction confidence scores were also considered during data interpretation. Toxicity predictions were used solely as preliminary computational indicators and not as definitive toxicological evidence [18,19].

2.5. Ligands and receptor preparation.

The selected ligands were downloaded from the PubChem database in Structure Data File (SDF) format and converted into Protein Data Bank (*.pdb) format using YASARA Structure. Energy minimization of ligands was performed using the YASARA "Energy Minimization" module with the AMBER14 force field. The crystal structure of superoxide dismutase was obtained from the RCSB Protein Data Bank under PDB ID: 2WYT. The protein corresponds to Cu/Zn superoxide dismutase derived from Homo sapiens. Chain A was selected for docking analysis because it contained the complete catalytic and predicted allosteric regions used in the study. The crystal structure resolution and structural information were verified from the PDB database before docking preparation. Protein preparation included the removal of crystallographic water molecules and non-essential co-crystallized ligands, while retaining the biologically relevant Cu^{2+} and Zn^{2+} ions required for structural and catalytic integrity. Hydrogen atoms were added according to physiological protonation states at neutral pH. Missing residues were evaluated during preprocessing, and no critical missing residues were identified within the selected docking region. The prepared receptor structure was subsequently minimized and saved in *.pdb format [20,21].

2.6. Molecular docking analysis.

Molecular docking simulations were conducted using YASARA (Yet Another Scientific Artificial Reality Application). Structure with the AutoDock VINA docking engine integrated through the dock_run.mcr and dock_runscreening.mcr macros developed by Elmar Krieger (http://www.yasara.org). Docking validation was performed using redocking to optimize grid-box parameters and assess reproducibility. The docking grid box was centered on the predicted allosteric pocket identified from ASD and AllositePro analyses. Docking calculations were performed using the VINA scoring method with 100 docking runs and the AMBER14 force field [21]. Multiple docking poses were generated for each ligand, and the final selected pose was determined based on docking score, interaction stability, hydrogen-bond interactions, and consistency with predicted allosteric-site residues. Docking score interpretation followed the YASARA scoring convention implemented in the VINA-based workflow. Because software-specific scoring conventions may differ from traditional negative

binding-energy representations, the docking values were interpreted comparatively within the same computational framework rather than as absolute thermodynamic measurements [21].

2.7. Data analysis.

Docking results and residue-interaction analyses were visualized in two-dimensional (2D) and three-dimensional (3D) formats using BIOVIA Discovery Studio Visualizer and PyMOL software. Complex structures generated in YASARA (*.yob) format were converted into *.pdb files for visualization and interaction analysis. Residue interactions, hydrogen bonds, hydrophobic contacts, electrostatic interactions, and metal-associated interactions were analyzed qualitatively to identify potential ligand-binding patterns near the predicted allosteric region of superoxide dismutase. Figures were generated with residue numbering, ligand labels, chain identifiers, and bond-distance annotations to improve interpretability and reproducibility [21].

3. Results and Discussion

The test ligands used in this research are 42 active compounds from *Peronema canescens Jack* and one comparison ligand, D-Trehalose [22,23]. Lipinski's Rule of 5 was the first physicochemical test performed. Out of 43 ligands, 4 ligands were eliminated. The remaining 39 ligands were evaluated using ADMET parameters, including Intestinal Absorption, Ames Toxicity, hERG Blockers, Carcinogenesis, and LD50. Out of 39 ligands tested, 13 ligands were eliminated, and the rest advanced to the next test stage. Virtual screening identified five test ligands with the lowest Gibbs free energy values. The five ligands were then docked with the receptor, and the results were compared to the D-trehalose docking result. The best ligands were then visualized and compared with D-Trehalose based on the interactions between the ligands and receptors.

3.1. Protein functional sites.

Functional-site analysis using the Conserved Domain Database (CDD) identified several conserved catalytic and metal-binding residues within SOD (PDB ID: 2WYT). The predicted catalytic residues included HIS46, HIS48, HIS63, HIS80, ASP83, and HIS120. The Cu^{2+}-binding residues were HIS46, HIS48, HIS63, and HIS120, whereas the Zn^{2+}-binding residues were HIS63, HIS71, HIS80, and ASP83, consistent with previous structural studies of Cu/Zn-SOD [24–26]. Prediction of putative allosteric regions using ASD and AllositePro identified several residues potentially associated with allosteric ligand interactions, including VAL5, CYS6, VAL7, LYS9, GLY10, ASP11, GLY51, ASP52, ASN53, THR54, ALA55, GLY56, CYS57, THR58, ALA60, THR116, SER142, ARG143, LEU144, CYS146, GLY147, and VAL148. These residues were subsequently used to define the docking region for targeted molecular docking analysis. However, it is important to emphasize that computational prediction of an allosteric pocket does not confirm functional allosteric regulation and requires experimental validation.

3.2. Pharmacokinetic test.

The Lipinski Rules of 5 (Table 1) are pharmacokinetic criteria that are quite important when conducting research around drug-like compounds. The Lipinski Rules of 5 include Molecular Weight, Log P, Rotatable Bonds, Donors and Acceptors, and Surface Area; if a

compound fails one or more of these rules, it can be predicted to have a bioavailability problem. Lipinski's rule describes the physicochemical properties of each compound based on predetermined criteria. [12]. Out of 43 ligands tested, 4 ligands were eliminated. The bioavailability radars of the top 5 ligands that passed the bioavailability test and D-Trehalose are shown in Figure 1.

Table 1. Results of Lipinski's rules of the 5 bioavailability test.

Ligand	Lipinski's Rules of 5					
	MW	**Log P**	**RB**	**H_A**	**H_D**	**TPSA**
Acceptable Value	≤ 500	≤ 5	≤ 10	≤ 10	≤ 5	≤ 140
D-Trehalose	342.3	-5.4	4	11	8	189.53
CHEMBL1407860	382.43	3.11	6	7	0	107.2
CHEMBL2440886	382.5	0.07	6	5	2	143.07
AKOS034376355	372.55	2.7	9	4	2	105.15
CHEMBL1539499	398.5	1.62	9	6	2	156.89
SCHEMBL4675593	194.16	-0.85	2	8	0	111.92

The remaining 39 ligands were evaluated using ADMET parameters, including Intestinal Absorption, AMES Toxicity, hERG Blockers, Carcinogenesis, and LD_{50} (Table 2). Out of 39 ligands tested, 13 ligands were eliminated, and the rest advanced to the next test stage. Virtual screening showed that, among the 26 test ligands, five compounds had the lowest Gibbs free energy values. The five ligands were then docked with the receptor, and the results were compared to the D-trehalose docking result. Table 2 described the result of several criteria selected from ADMET consist of Intestinal Absorption (>30% to be in the safe category), AMES Toxicity ("safe" result to enter the safe category), Human Ether-A-Go-Go Related Gene (hERG) blocker ("safe" result to enter the safe category) carcinogenesis ("Safe" result to enter the safe category), and LD_{50} (>300mg/KgBW/day to enter the safe category) [12,16,19].

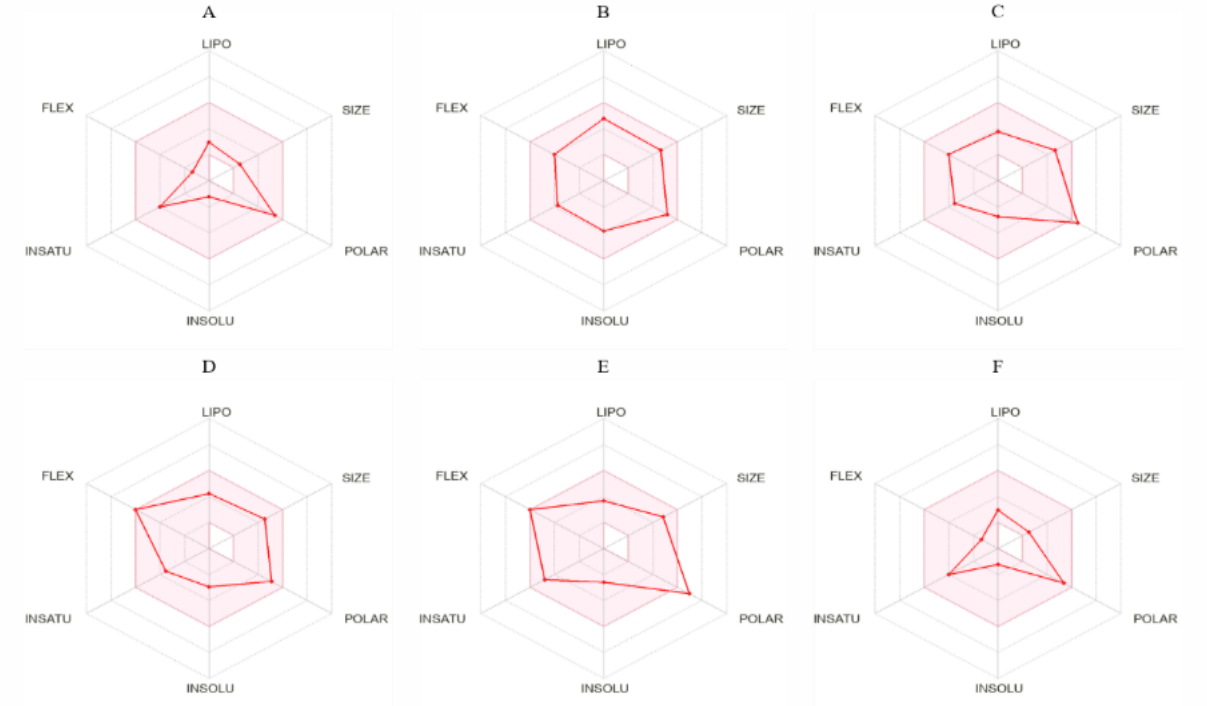

Figure 1. The bioavailability radars of **(A)** D-Trehalose; **(B)** CHEMBL1407860; **(C)** CHEMBL2440886; **(D)** AKOS034376355; **(E)** CHEMBL1539499; **(F)** SCHEMBL4675593.

Pharmacokinetic screening can be done using the criteria that have been created by Lipinski, which explains that the most "drug-like" molecules have a Log P value of ≤ 5, a molecular weight of ≤ 500, the number of hydrogen bond acceptors ≤ 10, the number of

hydrogen bond donors ≤ 5, and TPSA≤ 140 Å2. Molecules that violate one/more of these rules will have problems with bioavailability [27]. This rule is called the Rule of 5 because the basic values are 5, 500, 2x5, and 5. The fifth and sixth rules describe the numbers of donors and acceptors of hydrogen bonds (≤ 12) and of rotatable bonds (≤ 10). Drug absorption in the human body begins in the intestinal epithelium and ends at the site of drug action. Previous research has shown that compounds with a mass greater than 500 Daltons exhibit suboptimal absorption properties [27]. According to Table 1, all test ligands passed this test.

The second criterion is Log P, with a lipophilicity limit of Log P ≤ 5. Drug candidates that violate these criteria tend to be less soluble in physiological solutions and, therefore, cannot have access to the surface of the membrane. If the compound is too hydrophobic (Log P > 5), it will remain in the first membrane it contacts, and if it is too hydrophilic, it will never cross cell membranes to reach its site of action [27]. The number of donors and acceptors of hydrogen bonds has been shown to affect a molecule's physicochemical properties (solubility, absorption, distribution) and, in turn, a drug's efficacy. This indicates that, for better absorption and permeability, the number of donors and acceptors in the ligand should be less than 5 and 10, respectively. If the compound violates this criterion, it is too polar to pass through the cell membrane [27]. Based on Table 1, all the test ligands passed the lipophilicity test, but D-Trehalose failed the hydrogen-bond donor and acceptor count test.

Rotatable bond (Rot.Bond) is defined as any single non-ring bond, bounded to a non-terminal heavy (i.e., non-hydrogen) atom. Amide C-N bonds are not considered because of their high rotational energy barrier. This simple topological parameter measures molecular flexibility. It is a very good predictor of oral bioavailability [27]. According to Table 1, all test ligands passed this test. The TPSA of drug molecules has been reported to directly affect drug absorption across biological membranes, including CaCO-2 cells (large intestine carcinoma cells), brain cells, and nerve cells in the central nervous system. These studies reported that drugs with dynamic TPSA <60 Å2 are completely absorbed, whereas those with dynamic TPSA >140 Å2 exhibit restricted permeation [28]. Based on Table 1, D-Trehalose (CHEMBL2440886) and CHEMBL1539499 failed this test.

ADMET (Absorption, Distribution, Metabolism, Excretion, and Toxicity) is a set of criteria that influence the pharmacokinetic and pharmacodynamic effects of drug molecules. Calculating ADMET properties is very important for optimizing new drug molecules. Successful drug development must involve good ADMET properties in addition to good efficacy. Prediction of the fate of drugs and the effects caused by drugs in the body, such as how much of the drug is absorbed if given orally and how much is absorbed in the digestive tract, is an integral part of drug discovery. Similarly, if absorption is poor, its distribution and metabolism will be affected, potentially leading to neurotoxicity and nephrotoxicity. Ultimately, this research aims to understand the disposition of drug molecules in an organism. Thus, ADMET studies are among the most important parts of computational drug design [1,29].

A compound can reach a tissue if it enters the bloodstream. Usually, a drug is administered through mucous surfaces, such as the digestive tract, before it is taken up by target cells. Factors such as poor solubility of the compound, intestinal transit time, gastric emptying time, inability to permeate the intestinal wall, and chemical instability in the stomach contribute to reduced drug absorption after oral administration. Drugs with poor absorption are less desirable for oral administration, such as by inhalation or intravenously [1,12]. A molecule

with an Intestinal Absorption of less than 30% is considered poorly absorbed. According to Table 2, all test ligands passed this test.

Table 2. Results of ADMET test.

Ligand	ADMET				
	Intestinal Absorption	**AMES Toxicity**	**hERG Blockers**	**Hepatotoxicity**	**LD_{50}**
Acceptable Value	>0.3	Safe	Safe	No	≥300 mg/kg
D-Trehalose	0.98	Safe	Safe	No	2730 mg/kg
CHEMBL1407860	0.778	Safe	Safe	No	2730 mg/kg
CHEMBL2440886	0.964	Safe	Safe	No	1700 mg/kg
AKOS034376355	0.905	Safe	Safe	No	1000 mg/kg
CHEMBL1539499	0.84	Safe	Safe	No	1000 mg/kg
SCHEMBL4675593	0.98	Safe	Safe	No	395 0mg/kg

AMES toxicity is a widely used method for assessing the mutagenic potential of a drug in bacteria; when results are positive, the compound is considered mutagenic and may act as a carcinogen [12,16,19]. According to Table 2, all test ligands passed this test. The criteria for hERG inhibitors state that inhibition of the potassium channel encoded by the human ether-a-go-go gene (hERG) is the principal mechanism underlying QT prolongation and QT syndrome, which can cause dangerous ventricular arrhythmias [12]. According to Table 2, all test ligands passed this test. Drug-induced liver injury is a major safety concern for drug development and a significant cause of drug attrition. A compound is classified as hepatotoxic if it has at least one pathological or physiological liver event that is strongly associated with disrupted normal liver function. According to Table 2, all test ligands passed this test.

Toxicity analysis is very important for potential compounds. The lethal dose 50 (LD_{50}) is a standard measure of acute toxicity used to compare toxicity across molecules. LD_{50} is the amount of compound administered directly capable of causing the death of 50% of test animals. In ProTox-III, there are 6 classes of toxicity, in descending order, with the most fatal at the bottom. Classes for toxicity are based on the lower the LD_{50} value of any compound, with class 1 having an $LD_{50} \leq 5$ (fatal if consumed) and class 6 having an $LD_{50} > 5000$ (non-toxic) [16,19]. According to Table 2, all test ligands passed this test.

The remaining ligands were subsequently evaluated using ADMET criteria, including intestinal absorption, AMES toxicity, hERG inhibition, hepatotoxicity, and LD50 prediction (Table 2). The selected compounds generally showed favorable predicted intestinal absorption (>30%), non-mutagenic AMES profiles, absence of predicted hERG inhibition, non-hepatotoxic behavior, and acceptable predicted LD_{50} values. Nevertheless, these results should be interpreted with caution, as ADMET predictions from SwissADME, pkCSM, Deep-PK, and ProTox-III remain computational estimates that depend on their model training datasets and applicability domains.

3.3. Molecular docking between ligands and receptor.

Molecular docking was conducted using YASARA Structure with the AutoDock VINA scoring framework. The docking grid was centered on the predicted allosteric region identified by ASD and AllositePro analyses. Docking validation through redocking procedures was used to optimize grid parameters before ligand screening. The docking scores presented in this study follow the YASARA scoring convention, in which more positive values within the same computational framework indicate more favorable predicted binding interactions. Therefore, docking scores were interpreted comparatively rather than as absolute thermodynamic binding energies.

The docking results are summarised in Table 3. CHEMBL1407860 showed the highest docking score among the screened compounds (6.128 kcal/mol), followed by CHEMBL2440886 (5.961 kcal/mol), AKOS034376355 (5.757 kcal/mol), and CHEMBL1539499 (5.328 kcal/mol). D-trehalose exhibited a docking score of 5.183 kcal/mol. Lower predicted dissociation constants also suggested relatively stronger ligand binding within the docking model. Importantly, the docking results should be interpreted only as predicted binding affinity for the selected docking region, not as evidence of confirmed enzyme activation, therapeutic efficacy, or biological function. Molecular docking alone cannot demonstrate whether ligand binding enhances, inhibits, stabilizes, or destabilizes SOD activity.

Table 3. *Peronema canescens* Jack's molecular docking results in superoxide dismutase.

Ligand	Effi [kcal/(mol*Atom)]	Bind.energy[kcal/mol]	Dissoc. constant [pM]
D-Trehalose	0.2253	5.183	158785424.00
CHEMBL1407860	0.2357	6.128	32219326.00
CHEMBL2440886	0.2384	5.961	42709952.00
AKOS034376355	0.2399	5.757	60264708.00
CHEMBL1539499	0.2049	5.328	124315192
SCHEMBL4675593	0.3414	4.779	314012224.00

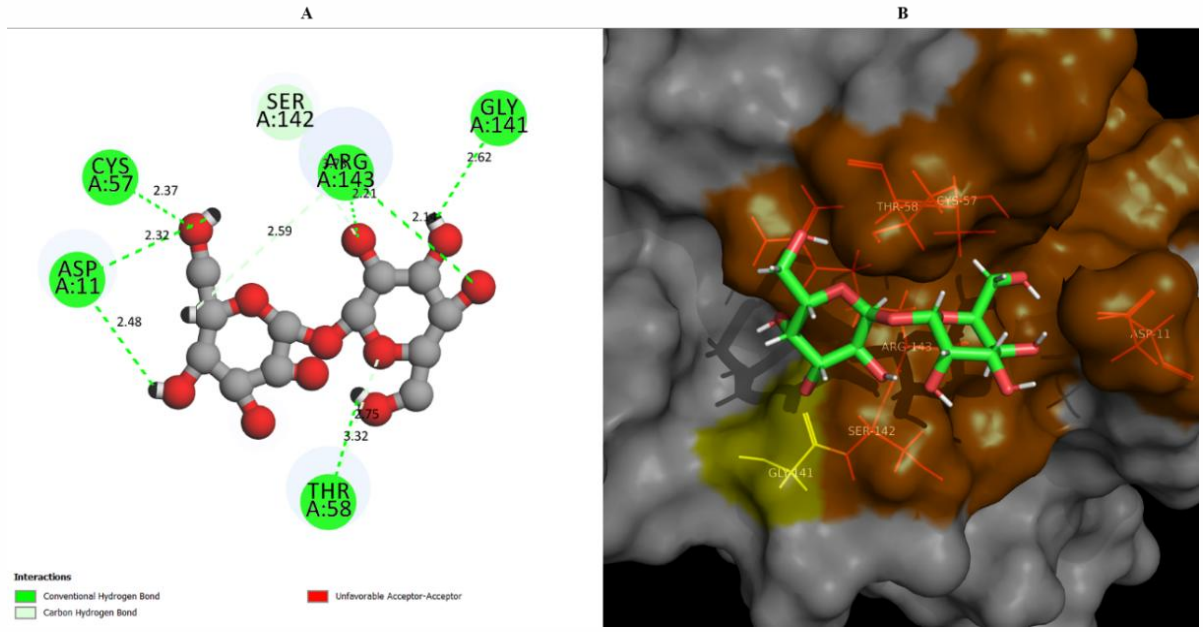

Figure 2. Receptor interactions with D-Trehalose.

The Grid box size used for screening is 1 Å, as it yielded an RMSD of 0.000 Å and a binding energy of 5.183 kcal/mol during redocking. This research provides screening results in the form of binding energy, residual contact, and interaction types. Table 3 presents the ranking of the top five ligands by binding energy. A positive score indicates the best binding energy in the YASARA structure. Thus, a higher score indicates better ligand binding to the receptor [21]. In addition, the interacting residues in this study are the same as those in the previous study, namely VAL7, LYS9, ASP11, ASN51, GLY54, CYS144, GLY145, and VAL146 [23]. Receptor interactions with D-Trehalose are shown in Figure 2, while receptor interactions with CHEMBL1407860 are shown in Figure 3.

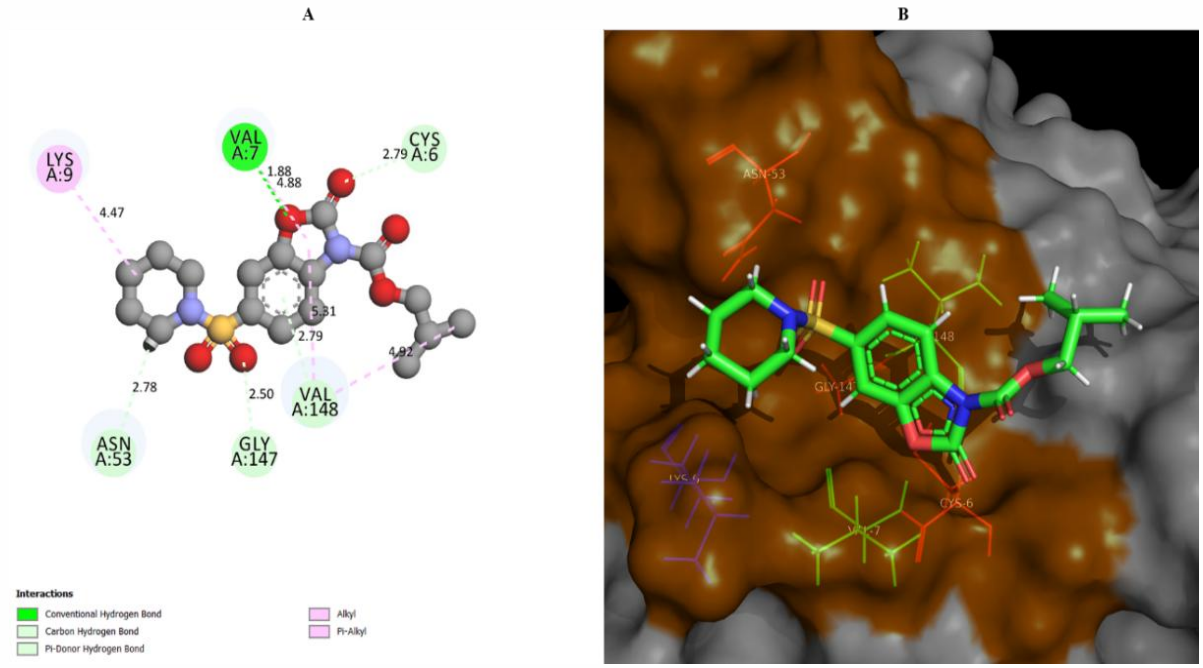

Figure 3. Receptor interactions with CHEMBL1407860.

Table 4 shows the interactions between each test ligand, divided into two categories: hydrogen bonds and hydrophobic bonds. The more hydrogen bonds a ligand has, hypothetically, the more easily and strongly it binds to the active site of the receptor. In contrast, hydrophobic bonds are considered important for stabilizing the interaction between ligands and receptors [30]. Molecular docking was performed to examine the interaction between the receptor and the ligand. The test ligands and receptors used are from the previous screening test. Molecular docking in this study was performed using a targeted docking approach focused on the allosteric sites.

Table 4. Residue interaction analysis between test ligands and superoxide dismutase.

Ligand	Residues/Amino acids involved	
	Hydrophobic interaction	**Hydrogen bond**
D-Trehalose		A ASP 11, A CYS 57, A THR 58, A GLY 141, A SER 142, A ARG 143
CHEMBL1407860	A VAL 7, A LYS 9, A VAL 148	A CYS 6, A VAL 7, A ASN 53, A GLY 147, A VAL 148
CHEMBL2440886	A LYS 9, A GLY 10,	A VAL 5, A VAL 7, A ASN 53, A VAL 148, A GLY 150
AKOS034376355	A VAL 148	A VAL 7, A LYS 9, A ASN 53, A CYS 146, A VAL 148
CHEMBL1539499	A LYS 9, A VAL 148	A VAL 7, A ASP 11, A ASN 53, A GLY 56, A CYS 146, A VAL 148
SCHEMBL4675593	A ARG 143	A THR 58, A GLY 141, A SER 142

The grid box size used for screening is 1 Å, as this yielded an RMSD of 0.000 Å and a binding energy of 5.18 kcal/mol during redocking. This research provides screening results in the form of binding energy, residual contact, and interaction types. The Superoxide Dismutase (SOD) (PDB: 2WYT) has several functional sites predicted by the Conserved Domain Database (CDD) server, including the conservation of the active-site residues HIS46, HIS48, HIS63, HIS80, ASP83, and HIS120. The conserved ion binding site were HIS46, HIS48, HIS63, HIS120 for Cu^{2+}) and HIS63, HIS71, HIS80, and ASP83 for Zn^{2+} [24-26]. The prediction result for allosteric site residue were VAL5, CYS6, VAL7, LYS9, GLY10, ASP11, GLY51, ASP52, ASN53, THR54, ALA55, GLY56, CYS57, THR58, ALA60, THR116, SER142, ARG143, LEU144, CYS146, GLY147, and VAL148 [10,15,17].

D-Trehalose was used as a binding energy control, so that the test ligand with a binding energy above D-Trehalose can be considered a potential ligand for development. Based on Table 3, the control ligand, D-Trehalose (CID_7427), has a binding energy of 5.183 kcal/mol. The test ligands with binding energies above D-Trehalose are CHEMBL1407860 (6.13 kcal/mol), CHEMBL2440886 (5.96 kcal/mol), AKOS034376355 (5.76 kcal/mol), and CHEMBL1539499 (5.33 kcal/mol). By sorting the best receptor-ligand complexes, YASARA identifies the best-scoring structure. Therefore, a score with a more positive result indicates a better binding of the ligand to the receptor [21]. In addition, a small Kd value indicates a stronger ligand binding to the receptor [20,21]. The ligand efficiencies of CHEMBL1407860 were 0.24, while D-Trehalose was 0.23, indicating that the binding energy contributed by each atom of the compounds was almost similar to the required energy to develop key contacts with the SOD target [21,31]. The range of ligand efficiency under D-Trehalose (based on binding energy) is 0.205 to 0.341 kcal/mol.

D-Trehalose (Figure 2) is the allosteric activator standard used in this study [22,23]. D-Trehalose forms two bonds with SOD, such as a conventional hydrogen bond and a carbon-hydrogen bond. A conventional hydrogen bond was formed at the amino acid residues ASP11, CYS57, THR58, GLY141, SER142, and ARG143. A carbon-hydrogen bond was formed at the amino acids THR58, SER142, and ARG143. The bond distances range from 2.14 to 3.73 Å.

CHEMBL1407860 (Figure 3) forms several bonds with SOD, such as a conventional hydrogen bond, a carbon-hydrogen bond, a pi-donor hydrogen bond, an alkyl bond, and a pi-alkyl bond. A conventional hydrogen bond was formed at the amino acid residue VAL7. A carbon-hydrogen bond was formed at the amino acids CYS6, ASN53, and GLY147. A pi-donor hydrogen bond was formed at the amino acid residue VAL148. An alkyl bond was formed at the amino acid residues LYS9 and VAL148. Pi-alkyl was formed at the amino acid residues VAL7 and VAL148. The bond distance formed varies from 1.88 to 5,31 Å.

Table 4 shows the interactions between each test ligand, divided into two categories: hydrogen bonds and hydrophobic bonds. The more hydrogen bonds the ligand has, hypothetically, the easier and stronger a ligand binds to the active side of the receptor. A good hydrogen bond has a distance less than 2.30 Å. Hydrophobic bonds are considered important because they stabilize interactions between ligands and receptors [30,32]. Based on Table 4, nearly all of the formed interaction bonds occurred in the allosteric site. Allostery refers to processes in which a binding event at one site of a biological macromolecule affects binding at another, distinct functional site, thereby regulating the corresponding function. Allosteric regulation has been recognized as playing a key role in many biological processes, most prominently in signal transduction, molecular machine function, transcriptional regulation, and metabolism [33].

Allostery is rooted in the fundamental physical properties of macromolecular systems and, probably, of other materials as well. Furthermore, allosteric effects are modulated by the cellular context in both health and disease. An allosteric activator is any molecule that binds to an enzyme's allosteric site and increases the activity of the enzyme. Because the interacting residues are mostly located within the predicted allosteric site, CHEMBL1407860 can serve as an alternative allosteric activator of Superoxide Dismutase, replacing D-Trehalose as a natural allosteric activator.

Residue-interaction analysis showed that several ligands interacted with residues located within or adjacent to the predicted allosteric region. CHEMBL1407860 formed hydrogen bonds and hydrophobic interactions involving residues CYS6, VAL7, ASN53,

GLY147, VAL148, and LYS9. These residues overlap with the computationally predicted allosteric-site residues identified during pocket analysis. However, interaction with predicted allosteric residues should not be interpreted as definitive evidence of functional allosteric regulation because computational contact analysis alone cannot determine conformational or catalytic consequences. Interestingly, several interacting residues identified for CHEMBL1407860 are located near structurally important regions of SOD, including regions associated with the electrostatic loop and dimer-interface stabilization. Binding near these regions could, in theory, influence protein flexibility, dimer stability, substrate accessibility, or local conformational dynamics. In addition, residues adjacent to metal-associated regions may indirectly contribute to the structural stabilization or destabilization of the enzyme. However, these possibilities remain speculative because no molecular dynamics simulations or experimental structural analyses were performed in the present study.

D-trehalose was included as a comparative reference ligand because previous studies suggested possible interactions with SOD-related antioxidant systems. In the present docking analysis, D-trehalose formed interactions involving ASP11, CYS57, THR58, GLY141, SER142, and ARG143. CHEMBL1407860 exhibited comparable interaction patterns within the predicted allosteric region and demonstrated a relatively favorable docking score within the YASARA framework. Nevertheless, these findings do not indicate that CHEMBL1407860 can replace D-trehalose or function as a confirmed natural allosteric activator. Hydrogen-bond interactions and hydrophobic contacts observed in the docking models may contribute to predicted ligand-binding stability. Short hydrogen-bond distances may indicate stronger local interactions, while hydrophobic contacts may contribute to stabilization of ligand orientation within the binding pocket [30,32]. However, docking-based interaction analysis represents a static computational approximation and does not account for protein flexibility, solvent effects, long-term conformational stability, or dynamic allosteric signaling. Therefore, additional validation studies are required before any mechanistic conclusions regarding SOD activation can be proposed. Molecular dynamics simulations, binding free-energy calculations, biochemical SOD activity assays, dose–response experiments, enzyme kinetic analyses, and cellular oxidative-stress studies are necessary to determine whether CHEMBL1407860 truly modulates SOD structure or function under biological conditions.

Additional structural interpretation of the docking results suggests that CHEMBL1407860 may interact with regions of superoxide dismutase (SOD) associated with structural stability and conformational regulation. Several interacting residues identified in the docking analysis, including VAL7, LYS9, ASN53, GLY147, and VAL148, are located near regions of the SOD dimer interface and the electrostatic loop. These structural regions are important for maintaining enzyme stability, substrate guidance, and catalytic efficiency in Cu/Zn-SOD proteins. The electrostatic loop region of SOD plays an important role in directing superoxide radicals toward the catalytic metal center through electrostatic interactions. Ligand binding near this region could potentially alter local conformational flexibility or influence substrate accessibility to the catalytic site. Depending on the nature of the interaction, such binding may theoretically contribute either to stabilization of the enzyme conformation or to structural perturbation that affects catalytic activity. Similarly, interactions occurring near the dimer interface may influence the stability of the SOD homodimer, which is essential for proper enzymatic function in Cu/Zn-SOD.

In addition, several predicted interaction residues are located adjacent to metal-associated regions involved in Cu^{2+} and Zn^{2+} coordination. Although CHEMBL1407860 was

not predicted to coordinate the catalytic metal ions directly, ligand binding near these structurally sensitive regions could potentially influence local hydrogen-bond networks, electrostatic interactions, or conformational dynamics surrounding the catalytic environment. Such effects might indirectly stabilize or destabilize the protein structure, thereby affecting enzyme activity. However, these structural interpretations remain hypothetical because the present study was limited to static molecular docking analysis. Molecular docking alone cannot determine whether ligand binding produces favorable conformational stabilization, dynamic allosteric signaling, or structural destabilization. Therefore, further studies involving molecular dynamics simulations, free-energy calculations, mutational analysis, and biochemical SOD activity assays are necessary to evaluate the functional consequences of CHEMBL1407860 binding and to determine whether the observed interactions contribute to enzyme modulation under biological conditions.

4. Conclusions

Based on the computational analyses conducted in this study, the bioactive compound CHEMBL1407860 derived from *Peronema canescens* demonstrated acceptable predicted pharmacokinetic and toxicity profiles and showed a higher docking score toward the predicted allosteric region of superoxide dismutase (SOD) compared with D-trehalose within the YASARA docking framework (6.13 kcal/mol vs 5.18 kcal/mol). Residue-interaction analysis suggested that CHEMBL1407860 may interact with residues associated with the predicted allosteric-binding region of SOD. However, the present findings are based solely on *in silico* computational prediction and do not confirm enzymatic activation or biological efficacy. Therefore, CHEMBL1407860 should be considered a computationally prioritized candidate for further investigation as a possible SOD allosteric-binding compound rather than a confirmed allosteric activator. Further validation studies, including molecular dynamics simulations, biochemical SOD activity assays, dose–response analysis, enzyme kinetic studies, and cellular oxidative-stress assays, are necessary to evaluate its mechanism of action, binding stability, and potential biological relevance.

Author Contributions

Conceptualization, M.M.A.H., D.A., and R.H.B.S.; methodology, D.A. and R.H.B.S.; formal analysis, M.M.A.H., D.A., and R.H.B.S.; data curation, M.M.A.H.; writing—original draft preparation, M.M.A.H., D.A., and R.H.B.S.; writing—review and editing, M.M.A.H., D.A., and R.H.B.S. All authors contributed equally to this work and have read and agreed to the published version of the manuscript.

Institutional Review Board Statement

Not applicable.

Informed Consent Statement

Not applicable.

Data Availability Statement

Data supporting the findings of this study are available upon reasonable request from the corresponding author.

Funding

This research received no external funding.

Acknowledgments

The author would like to thank all parties who have contributed to the completion of this research. All authors made equal contributions as the main contributors to this manuscript. No funding resources were reported for this publication.

Conflicts of Interest

The authors declare no conflict of interest.

Role of Funders

The funders had no role in the design of the study, the collection, analysis, or interpretation of data, the writing of the manuscript, or the decision to publish the results.

Abbreviations

The following abbreviations are used in this manuscript:

Abbreviation	Definition
ROS	Reactive Oxygen Species
ADMET	Absorption, Distribution, Metabolism, Excretion, and Toxicity
SAR	Structure Activity Relationship
YASARA	Yet Another Scientific Artificial Reality Application
LD_{50}	Lethal Dose 50
CDD	Conserved Domain Database
TPSA	Topological Polar Surface Area
SOD	Superoxide Dismutase

References

1. Flores-Holguín, N.; Frau, J.; Glossman-Mitnik, D. *In silico* Pharmacokinetics, ADMET Study and Conceptual DFT Analysis of Two Plant Cyclopeptides Isolated From Rosaceae as a Computational Peptidology Approach. *Front. Chem.* **2021**, *9*, 708364, https://doi.org/10.3389/fchem.2021.708364.
2. Hasan, A.E.Z.; Safithri, M.; Huda, A.S.; Kurniasih, R. *In silico*, to Determine The Active Compounds of Black Tea and Turmeric In Increasing The Activity of The Enzyme Sod. *Indones. J. Appl. Res.* **2022**, *3*, 32-45, http://dx.doi.org/10.30997/ijar.v3i1.187.
3. Azadmanesh, J.; Trickel, S.R.; Borgstahl, G.E.O. Substrate-analog binding and electrostatic surfaces of human manganese superoxide dismutase. *J. Struct. Biol.* **2017**, *199*, 68-75, https://doi.org/10.1016/j.jsb.2017.04.011.
4. Strange, R.W.; Antonyuk, S.; Hough, M.A.; Doucette, P.A.; Rodriguez, J.A.; Hart, P.J.; Hayward, L.J.; Valentine, J.S.; Hasnain, S.S. The Structure of Holo and Metal-deficient Wild-type Human Cu, Zn Superoxide Dismutase and its Relevance to Familial Amyotrophic Lateral Sclerosis. *J. Mol. Biol.* **2003**, *328*, 877-891, https://doi.org/10.1016/s0022-2836(03)00355-3.
5. Fransisca, D.; Kahanjak, D.N.; Frethernety, A. Uji aktivitas antibakteri ekstrak etanol daun sungkai (Peronema canescens Jack) terhadap pertumbuhan Escherichia coli dengan metode difusi cakram Kirby-Bauer. *J. Pengelolaan Lingkung. Berkelanjutan* **2020**, *4*, 460–470, http://dx.doi.org/10.36813/jplb.4.1.460-

470.
6. Yani, A.P.; Putranto, A.M.H. Examination of the Sungkai's young leaf extract (Peronema Canescens) as an antipiretic, immunity, antiplasmodium and teratogenity in mice (Mus. muculus). *Int. J. Sci. Eng.* **2014**, *7*, 30-34, https://doi.org/10.12777/ijse.7.1.30-34.
7. Latief, M.; Sari, P.M.; Fatwa, L.T.; Tarigan, I.L.; Rupasinghe, H.P. Antidiabetic activity of sungkai (Peronema canescens Jack) leaves ethanol extract on the male mice induced alloxan monohydrate. *Pharmacol. Clin. Pharm. Res.* **2021**, *6*, 64, https://doi.org/10.15416/pcpr.v6i2.31666.
8. Pindan, N.P.; Daniel; Saleh, C.; Magdaleni, A.R. Phytochemical test and antioxidant activity test of n-hexane fraction extract, ethyl acetate and remained ethanol from leaf of sungkai (*Peronema canescens jack*.) using DPPH method. *Jurnal Atomik*. **2021**, *6*, 22–27, https://jurnal.kimia.fmipa.unmul.ac.id/index.php/JA/article/view/815/632
9. Carolina, M.; Araya, W.; Carolina, P.; Iskandar, D.P. Efektifitas Pemberian Seduhan Daun Sungkai (Peronema canescens Jack) Terhadap Perubahan Tekanan Darah Pada Lansia Hipertensi Di Wilayah Upt Puskesmas Pahandut Palangka Raya. *J. Kesehat. Tambusai* **2022**, *3*, 442-452, https://doi.org/10.31004/jkt.v3i3.6448.
10. Huang, W.; Lu, S.; Huang, Z.; Liu, X.; Mou, L.; Luo, Y.; Zhao, Y.; Liu, Y.; Chen, Z.; Hou, T.; Zhang, J. Allosite: a method for predicting allosteric sites. *Bioinformatics* **2013**, *29*, 2357-2359, https://doi.org/10.1093/bioinformatics/btt399.
11. Marchler-Bauer, A.; Derbyshire, M.K.; Gonzales, N.R.; Lu, S.; Chitsaz, F.; Geer, L.Y.; Geer, R.C.; He, J.; Gwadz, M.; Hurwitz, D.I.; Lanczycki, C.J.; Lu, F.; Marchler, G.H.; Song, J.S.; Thanki, N.; Wang, Z.; Yamashita, R.A.; Zhang, D.; Zheng, C.; Bryant, S.H. CDD: NCBI's conserved domain database. *Nucleic Acids Res.* **2015**, *43*, D222-D226, https://doi.org/10.1093/nar/gku1221.
12. Pires, D.E.V.; Blundell, T.L.; Ascher, D.B. pkCSM: Predicting Small-Molecule Pharmacokinetic and Toxicity Properties Using Graph-Based Signatures. *J. Med. Chem.* **2015**, *58*, 4066-4072, https://doi.org/10.1021/acs.jmedchem.5b00104.
13. Marchler-Bauer, A.; Bo, Y.; Han, L.; He, J.; Lanczycki, C.J.; Lu, S.; Chitsaz, F.; Derbyshire, M.K.; Geer, R.C.; Gonzales, N.R.; Gwadz, M.; Hurwitz, D.I.; Lu, F.; Marchler, G.H.; Song, J.S.; Thanki, N.; Wang, Z.; Yamashita, R.A.; Zhang, D.; Zheng, C.; Geer, L.Y.; Bryant, S.H. CDD/SPARCLE: functional classification of proteins via subfamily domain architectures. *Nucleic Acids Res.* **2017**, *45*, D200-D203, https://doi.org/10.1093/nar/gkw1129.
14. Daina, A.; Michielin, O.; Zoete, V. SwissADME: a free web tool to evaluate pharmacokinetics, drug-likeness and medicinal chemistry friendliness of small molecules. *Sci. Rep.* **2017**, *7*, 42717, https://doi.org/10.1038/srep42717.
15. Song, K.; Liu, X.; Huang, W.; Lu, S.; Shen, Q.; Zhang, L.; Zhang, J. Improved Method for the Identification and Validation of Allosteric Sites. *J. Chem. Inf. Model.* **2017**, *57*, 2358-2363, https://doi.org/10.1021/acs.jcim.7b00014.
16. Banerjee, P.; Dehnbostel, F.O.; Preissner, R. Prediction Is a Balancing Act: Importance of Sampling Methods to Balance Sensitivity and Specificity of Predictive Models Based on Imbalanced Chemical Data Sets. *Front. Chem.* **2018**, *6*, 362, https://doi.org/10.3389/fchem.2018.00362.
17. Liu, X.; Lu, S.; Song, K.; Shen, Q.; Ni, D.; Li, Q.; He, X.; Zhang, H.; Wang, Q.; Chen, Y.; Li, X.; Wu, J.; Sheng, C.; Chen, G.; Liu, Y.; Lu, X.; Zhang, J. Unraveling allosteric landscapes of allosterome with ASD. *Nucleic Acids Res.* **2020**, *48*, D394-D401, https://doi.org/10.1093/nar/gkz958.
18. Alazmi, M.; Motwalli, O. *In silico* virtual screening, characterization, docking and molecular dynamics studies of crucial SARS-CoV-2 proteins. *J. Biomol. Struct. Dyn.* **2021**, *39*, 6761–6771, https://doi.org/10.1080/07391102.2020.1803965.
19. Banerjee, P.; Kemmler, E.; Dunkel, M.; Preissner, R. ProTox 3.0: a webserver for the prediction of toxicity of chemicals. *Nucleic Acids Res.* **2024**, *52*, W513-W520, https://doi.org/10.1093/nar/gkae303.
20. Aamir, M.; Singh, V.K.; Dubey, M.K.; Meena, M.; Kashyap, S.P.; Katari, S.K.; Upadhyay, R.S.; Umamaheswari, A.; Singh, S. *In silico* Prediction, Characterization, Molecular Docking, and Dynamic Studies on Fungal SDRs as Novel Targets for Searching Potential Fungicides Against Fusarium Wilt in Tomato. *Front. Pharmacol.* **2018**, *9*, 1038, https://doi.org/10.3389/fphar.2018.01038.
21. Gholam, G.M.; Irsal, R.A.P.; Dwicesaria, M.A.; Hasibuan, M.M.A. *In silico* Study of Combined Docking and Molecular Dynamics Simulation for Hops (*Humulus lupulus*) Active Compounds in Inhibiting Duffy-Binding Protein (DBP) as Anti-*Plasmodium vivax* (*P. vivax*). *Proceedings* **2024**, *103 (1)*, 66, https://doi.org/10.3390/proceedings2024103066.

22. Ma, X.; Deng, D. Inhibitors and Activators of SOD, GSH-Px, and CAT. In Enzyme Inhibitors and Activators, Şentürk, M., Ed.; IntechOpen: London, **2017**; https://doi.org/10.5772/65936.
23. Putri, R.S.; Safithri, M.; Ardianto, D. Active Compound of Red Betel (Piper Crocatum Ruiz & Pav) as Activator of Cu/Zn Superoxide Dismutase *in silico*. *Indones. J. Appl. Res.* **2022**, *3*, 85–94.
24. Banci, L.; Bertini, I.; Cramaro, F.; Del Conte, R.; Viezzoli, M.S. The solution structure of reduced dimeric copper zinc superoxide dismutase. *Eur. J. Biochem.* **2002**, *269*, 1905-1915, https://doi.org/10.1046/j.1432-1033.2002.02840.x.
25. Bordo, D.; Djinovic, K.; Bolognesi, M. Conserved Patterns in the Cu,Zn Superoxide Dismutase Family. *J. Mol. Biol.* **1994**, *238*, 366-386, https://doi.org/10.1006/jmbi.1994.1298.
26. Bourne, Y.; Redford, S.M.; Steinman, H.M.; Lepock, J.R.; Tainer, J.A.; Getzoff, E.D. Novel dimeric interface and electrostatic recognition in bacterial Cu,Zn superoxide dismutase. *Proc. Natl. Acad. Sci. U.S.A.* **1996**, *93*, 12774-12779, https://doi.org/10.1073/pnas.93.23.12774.
27. Vishnu Kumar, S.; Rajesh Kumar, S.; Pashupati Prasad, S. Extended Rule of Five and Prediction of Biological Activity of peptidic HIV-1-PR Inhibitors. *Univ. J. Pharm. Pharmacol.* **2022**, *1*, 20, https://doi.org/10.31586/ujpp.2022.403.
28. Karami, T.K.; Hailu, S.; Feng, S.; Graham, R.; Gukasyan, H.J. Eyes on Lipinski's Rule of Five: A New "Rule of Thumb" for Physicochemical Design Space of Ophthalmic Drugs. *J. Ocul. Pharmacol. Ther.* **2022**, *38*, 43-55, https://doi.org/10.1089/jop.2021.0069.
29. Chandrasekaran, B.; Abed, S.N.; Al-Attraqchi, O.; Kuche, K.; Tekade, R.K. Chapter 21 - Computer-Aided Prediction of Pharmacokinetic (ADMET) Properties. In Dosage Form Design Parameters, Tekade, R.K., Ed.; Academic Press: **2018**; Volume 2, pp. 731-755, https://doi.org/10.1016/B978-0-12-814421-3.00021-X.
30. Putera Irsal, R.A.; Hami Seno, D.S.; Safithri, M.; Kurniasih, R. PENAPISAN VIRTUAL SENYAWA AKTIF SIRIH MERAH (Piper Crocatum) SEBAGAI INHIBITOR ANGIOTENSIN CONVERTING ENZYME. *J. Farmamedika* **2022**, *7*, 104-113, https://doi.org/10.47219/ath.v7i2.157.
31. Patel, C.N.; Goswami, D.; Jaiswal, D.G.; Parmar, R.M.; Solanki, H.A.; Pandya, H.A. Pinpointing the potential hits for hindering interaction of SARS-CoV-2 S-protein with ACE2 from the pool of antiviral phytochemicals utilizing molecular docking and molecular dynamics (MD) simulations. *J. Mol. Graph. Model.* **2021**, *105*, 107874, https://doi.org/10.1016/j.jmgm.2021.107874.
32. Uzzaman, M.; Hasan, M.K.; Mahmud, S.; Yousuf, A.; Islam, S.; Uddin, M.N.; Barua, A. Physicochemical, spectral, molecular docking and ADMET studies of Bisphenol analogues; A computational approach. *Inform. Med. Unlocked* **2021**, *25*, 100706, https://doi.org/10.1016/j.imu.2021.100706.
33. Wodak, S.J.; Paci, E.; Dokholyan, N.V.; Berezovsky, I.N.; Horovitz, A.; Li, J.; Hilser, V.J.; Bahar, I.; Karanicolas, J.; Stock, G.; Hamm, P.; Stote, R.H.; Eberhardt, J.; Chebaro, Y.; Dejaegere, A.; Cecchini, M.; Changeux, J.-P.; Bolhuis, P.G.; Vreede, J.; Faccioli, P.; Orioli, S.; Ravasio, R.; Yan, L.; Brito, C.; Wyart, M.; Gkeka, P.; Rivalta, I.; Palermo, G.; McCammon, J.A.; Panecka-Hofman, J.; Wade, R.C.; Di Pizio, A.; Niv, M.Y.; Nussinov, R.; Tsai, C.-J.; Jang, H.; Padhorny, D.; Kozakov, D.; McLeish, T. Allostery in Its Many Disguises: From Theory to Applications. *Structure* **2019**, *27*, 566-578,, https://doi.org/10.1016/j.str.2019.01.003.

Publisher's Note & Disclaimer

Supplementary Materials

Table S1. Bioactive compounds contained in sungkai leaves.

Compound number	Compound	Synonym
1	ethyl phosphate	CHEBI:59760
2	decanoic acid	SMR001252255
3	dodecanoic acid	SMR001253907
4	1–hexadecanol	CHEBI:16125
5	5–octadecene	DTXSID70880871
6	hexadecene	DTXSID1027269
7	hexadecane	DTXSID0027195
8	isopropyl myristate	DTXSID0026838
9	tetradecanoic acid	DTXSID6021666
10	hexadecanoic acid	DTXSID2021602
11	methyl 11-octadecenoate	SCHEMBL123511
12	2–nonadecanone	DTXSID70212077
13	2-propenyl decanoate	DTXSID5069209
14	1–eicosanol	DTXSID0027272
15	9–octadecanone	DTXSID90334068
16	1,2-benzenedicarboxylic acid	DTXSID8021484
17	12–tricosanone	DTXSID4060238
18	heptacosane	DTXSID6058637
19	tetratetracontane	DTXSID5058640
20	Ethyl 2-benzylidene-3-oxobutanoate	DTXSID101337851
21	Caffeine	DTXSID0020232
22	L-(+)-Valine	DTXSID40883233
23	N, N-dihydroxy-3,5-dinitro-1,3,5-triazinan-1-amine	SCHEMBL13963031
24	1-Morpholin-4-yl-2-(4-nitro-pyrazol-1-yl)-ethanone	AKOS001734994
25	3,4,5-Trimethoxycinnamate	CHEBI:58949
26	2S)-N-(5-Chloro-1,3-thiazol-2-yl)-2-[4-(methylsulfonyl)-2-oxo-1-piperazinyl]-3-(tetrahydro-2H-pyran-2-yl)propanamide	CHEMBL2346880
27	Thiophene, 2-(9,9'-spirobi[9H-fluoren]-2-yl)-	DTXSID50454478
28	2-[[4-amino-5-[3-(diethylsulfamoyl)phenyl]-1,2,4-triazol-3-yl]sulfanyl]-N-methylacetamide	CHEMBL1539499
29	1-[3-(Dimethylamino)-2,2-dimethylpropyl]-3-[3-(dimethylsulfamoyl)phenyl]thiourea	AKOS034376355
30	2-Oxo-6-(piperidine-1-sulfonyl)-benzooxazole-3-carboxylic acid isobutyl ester	CHEMBL1407860
31	2-({2-[4-(2-Hydroxyethyl)-1-piperazinyl]-2-oxoethyl}sulfanyl)-5,6-dimethylthieno[2,3-d]pyrimidin-4(3H)-one	CHEMBL2440886
32	N-[2-[2-(2-aminoethylamino)ethylamino]ethyl]-2-[1-[2-(2-aminoethylamino)ethyl]-4,5-dihydroimidazol-2-yl]acetamide	SCHEMBL14003712
33	2-Aminopalmitic acid	CHEMBL210903
34	Ethyl 6-methyl-2-thioxo-4-(3,4,5-trimethoxyphenyl)-1,2,3,4-tetrahydropyrimidine-5-carboxylate	AKOS000286607
35	Prednisone	DTXSID4021185
36	2-Hexyl-3,5-dipentylpyridine	DTXSID40423971
37	N-Isobutyl-N-[4-methoxyphenylsulfonyl]glycyl hydroxamic acid	CHEMBL311932
38	(2S)-2,6-diamino-N-[3-[3-[[(2S)-2,6-diaminohexanoyl]amino]propyl-methylamino]propyl]hexanamide	SCHEMBL22214538
39	2-Ethylhexyl 5-{8-[(2-ethylhexyl)oxy]-8-oxooctyl}-2-hexyl-3-cyclohexene-1-carboxylate	DTXSID20887072
40	glycidyl oleate	DTXSID101031637
41	Bis(1-methyltetrazol-5-yl)diazene	CHEMBL4675593
42	Methyl alpha-D-mannopyranoside	DTXSID10897266ss